Molecular Engineering of Hybrid Dye−Silica Fluorescent Nanoparticles: Influence of the Dye Structure on the Distribution of Fluorophores and Consequent Photoemission Brightness

Molecular engineering of hybrid dye-silica fluorescent nanoparticles: influence of the dye structure on the distribution of fluorophores and consequent photoemission brightness

Gabriele Alberto,[*,†,§] Giuseppe Caputo,[†,§] Guido Viscardi, [†,§] Salvatore Coluccia [†,§] and Gianmario Martra [*,†,§]

[†] Department of Chemistry, University of Torino, via P. Giuria 7, 10125 Torino, Italy

[§] NIS (Nanostructured Interfaces and Surfaces) Interdepartmental Centre of Excellence, at the Centre for Innovation, via G. Quarello 11/a, 10135, Torino, Italy

KEYWORDS. fluorescent silica nanoparticles, photoemission brightness, microemulsion, fluorophore hydrophilicity

ABSTRACT: This work was addressed to the elucidation of molecular parameters that rule the distribution of organic fluorophores throughout the nascent inorganic network during the synthesis of hybrid dye-silica nanoparticles by the reverse microemulsion method, that involves the partition of reactants among bulk oil phase, surfactant palisade and inner water core. The evolution of the photophysical properties (absorption, steady state and time-resolved photoluminescence) of three cyanine dyes, differing for the number of sulfonic substituents, from the starting microemulsion to the final nanoparticles provided evidence of the key role of the hydrophilicity of the fluorophores in ruling the dispersion within the SiO_2 matrix.

INTRODUCTION

Luminescence is widely exploited in systems and devices employed in several fields such as photonics,[1,2] optoelectronics,[3,4] chemical sensing,[5,6] life science (biology, biotechnology, biomedicine)[7,8] and forensic sciences.[9,10] In particular, photoluminescence plays an important role in these fields because of the ease of excitation (light) and the large number of photoluminescent compounds that are commercially available.

Throughout the past two decades, traditional organic fluorescent probes have been gradually replaced by photoluminescent nanomaterials, such as quantum dots[11,12] and hybrid nanoparticles (NPs), that are generated by the inclusion of fluorescent compounds in organic[13,14] or inorganic solid[15,16] or porous[17] matrices. In all cases, improved brightness and photostability have been attained, both of which are appealing for technological applications. Among the hybrid NPs based on inorganic matrices, dye-doped silica NPs play a particularly special role for two reasons. First, their preparation methods are knowledge based, which allows for the size control (and size homogeneity) of the NPs[18,19] and is the basis for further developments aimed toward innovative, smart targets. Additionally, the NPs are highly compatible with biological systems, which renders them attractive for in vivo imaging and therapy.[20,21] Indeed, amorphous silica is non-toxic,[22] although nanotoxicologists are investigating the possible adverse effects of this material in nanoform.

With respect to the effectiveness of dye doping a silica matrix, the seminal works of Santra et al.[23] and Van Blaaderen et al.[24,25] indicate that the fluorophore can be simply added as such or derivatized with an alkoxysilane moiety, respectively. Independently of the fluorophore and the preparation method, the performance of the final nanomaterial is determined to a significant extent by the distribution of the photoluminescent molecules within the host matrix because intermolecular quenching effects can occur.

In the case of hybrid luminescent silica NPs prepared by the so-called Stöber method, which exploits the hydrolysis of alcoxides and the polycondensation of the products in a homogeneous solution,[26] Rampazzo et al. demonstrated the spontaneous accumulation of dye molecules (namely, a pyrene-alcoxysilane derivative) in the core of a silica matrix.[27]

Furthermore, Larson et al.[28] were successful in tailoring the material architecture from a compact core-shell structure to an expanded core-shell structure and finally to homogeneously dye-doped SiO_2 NPs (where the dye was a rhodamine derivative) by changing the timing of the addition of the silica precursors with respect to the condensation of dye molecules derivatized with 3-aminopropyltriethoxysilane. However, in the case of simultaneous presence of the molecular precursor of silica and dye-silane derivatives, is it possible to control the distribution of fluorophores within the siliceous network by playing with some of the fluorophores physical-chemical characteristics?

To answer this question, we consider the possibility of preparing nanometer-sized silica by using the microemulsion method, wherein the hydrolysis of alcoxides and subsequent polycondensation occur in the “water pools” of reverse micelles.[29] Usually, this method is less favorable with respect to the Stöber-Van Blaaderen synthesis because of its higher procedural complexity, but allowances can typically be made to obtain quite narrow particle-size distributions.[30] A comprehensive study of the role of microemulsion parameters on the features of silica NPs doped with Ru(bpy) was performed by Bagwe et al.,[31] and in previous studies we also reported that indocarbocyanine dyes (which are of interest for many applications)[32] can be effectively entrapped in SiO_2 NPs.[33] Notably, the type of cyanine employed was not significantly soluble in water, which contrasted with the general idea that the microemulsion method, which is characterized by the nucleation and growth of the siliceous network in “water pools”, could be more effective for the entrapment of hydrophilic fluorophores.[34] Indeed, the multiphasic character of the reverse microemulsion, with the surfactant “palisade” separating the water pool from the bulk oil phase, and the consequent partition in different phases of the molecular species involved in the formation of the hybrid material stimulated in the investigation of the role of the hydrophilicity of a dye in determining its dispersion in the final hybrid NPs. The goal was the identification of a molecular parameter that, among other features, could effectively help to tailor the photophysical performance of hybrid dye-silica NPs.

Thus, a systematic investigation based on the use of three types of cyanine derivatives differing only in the number of sulfonic groups (see Chart 1) was performed by monitoring the fate of fluorophores from the initial microemulsion to the final hybrid material. On the basis of previous studies,[33] photoluminescence spectroscopy in the steady-state and time-resolved modes was employed, augmented by absorption electronic spectroscopy and complementary methods for a quantitative description of the prepared nanomaterials.

Chart 1. Molecular structures of I3BS-APTS (a), I3MS-APTS (b) and I3NS-APTS (c)

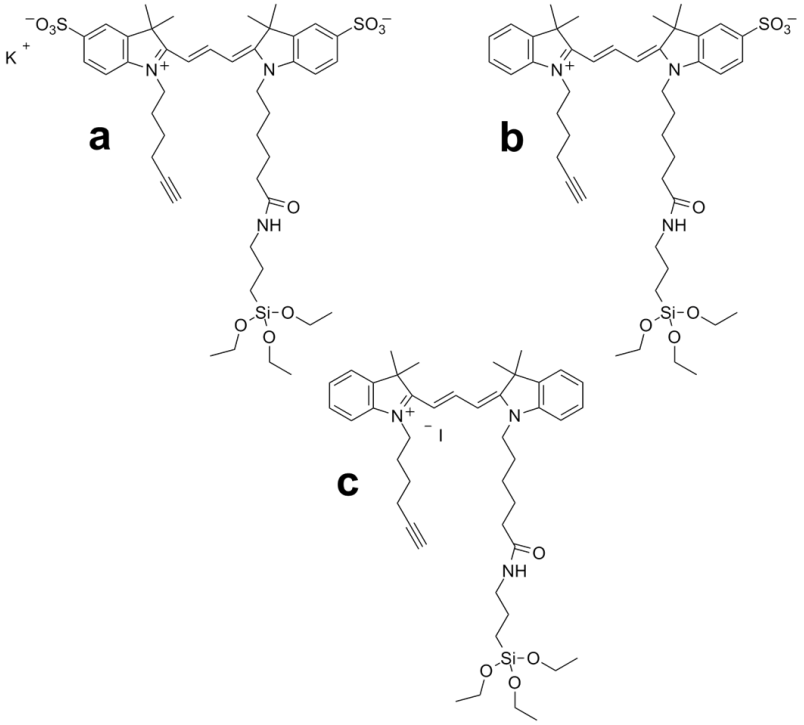

EXPERIMENTAL SECTION

Materials. N-hydroxysuccinimide (NHS) esters of bi/mono/not- sulfonated commercial cyanines IRIS3 (hereafter I3BS, I3MS, and I3NS, respectively, Chart S1 in the Supporting Information) were purchased from Cyanine Technologies SpA (Torino, Italy). All other reagents and solvents (tetraethylorthosilicate, aminopropyltriethoxysilane, cyclohexane, n-hexanol, Triton X-100, methanol, ethanol, dimethylformamide, acetonitrile, diethylether) were high-purity Sigma-Aldrich products and used as received.

Synthesis of Cyanine−Silane Derivatives. Cyanine-amino- propyltriethoxysilane derivatives (Chart 1) were prepared by adding aminopropyltriethoxysilane (APTS, 46.0 μmol, 10 μL) to a cyanine NHS-ester solution in dimethylformamide (11.5 μmol in 500 μL of DMF) and stirring for 24 h at room temperature. The reaction was monitored by thin-layer chromatography (TLC) and mass spectrometry (MS) for the complete conversion of the NHS esters in cyanine-APTS. The final products were finally separated from the unreacted APTS by dilution in diethylether and subsequent filtration to obtain powders as products.

Reverse Phase (RP)-HPLC Analyses. Reverse phase high pressure liquid chromatography (RP-HPLC) analyses were performed with a Waters 1525 HPLC instrument equipped with a 2996 photodiode array detector. Chromatographic separation was performed using a Waters SunFire C8 column (5 μm, 4.6 × 250 mm) at flow rate of 0.8 mL/min, constant temperature of 25 °C, and detection wavelength of 459 nm. The mobile phases were water + 0.1% trifluoroacetic acid (TFA) and acetonitrile + 0.1% TFA for pump A and pump B, respectively. Analyses were performed under isocratic conditions for the first 10 min A (v/v)/B (v/v) = 67.5/32.5 and gradient conditions for 20 min up to A (v/v)/B (v/v) = 30/70. The samples were diluted in methanol; the injection volume was set to 10 μL.

Preparation of Cyanine-Loaded Silica NPs. Fluorescent silica NPs doped with each of the three cyanine-APTS derivatives were synthesized by using a W/O microemulsion method, which has been well established in the literature.[24,35] Depending on the cyanine-APTS derivative, the three nanomaterials will be hereafter referred to as I3BS-NPs, I3MS-NPs, and I3NS-NPs. The microemulsion environment was prepared by mixing cyclohexane, *n*-hexanol, Triton X-100, and deionized water according to the relative quantities reported in Table 1.

Table 1. Microemulsion composition

Microemulsion Component	Volume (mL)	Moles	Molar Ratio
Water	5.40	0.3	1.00
Cyclohexane	75.00	0.69	0.43
n-hexanol	18.00	0.14	2.09
Triton X-100	17.70	0.03	10.00

The mixture was gently stirred at room temperature for 30 min, and the appropriate cyanine-APTS derivative (0.6 μmol, 0.2 mL) was then added. After stirring for 10 min, TEOS (4.5 mmol, 1 mL) and NH_4OH (28−30%, 5.3 mmol, 0.7 mL) were added to initiate the hydrolysis and polycondensation of the silane species. The reaction mixture was stirred for 24 h at room temperature, and the reaction was then interrupted by the addition of acetone (40 mL). The NPs were separated from the supernatant by centrifugation and were then washed twice with absolute ethanol and several times with deionized water to completely remove surfactant molecules. The samples were finally resuspended in deionized water and stored at room temperature. The supernatants and washing solvents were also investigated for the presence of unreacted dye molecules by UV−vis spectrophotometry.

Transmission Electron Microscopy (TEM). TEM images were obtained with a 3010 Jeol instrument operating at 300 kV. For the measurements, a droplet of the suspended IRIS3-NPs was spread on a copper grid coated with a perforated

carbon film, and the liquid was then allowed to evaporate slowly to limit the aggregation of NPs. The histogram of the size distribution of NPs was obtained by measuring ca. 300 particles, and the mean diameter (d_m) was calculated as $dm=\sum d_i n_i / \sum n_i$, where n_i is the number of particles of diameter d_i. The results are expressed as ($d_m \pm$ STDV).

UV−Vis Absorption Spectroscopy. Electronic absorption spectra were collected with a Varian Cary 5000 spectrophotometer. In the case of dried NPs samples, an integrating sphere coated with Spectralon (also used as reference) was inserted for measurements in the diffuse- reflectance mode. The reflectance spectra were then converted to absorbance-like profiles by using the Kubelka−Munk function.

Photoluminescence Spectroscopy. Photoemission/excitation steady-state spectra and fluorescence lifetimes were acquired with a Horiba Jobin Yvon Fluorolog 3 TCSPC spectrofluorimeter equipped with a 450-W Xenon lamp and a Hamamatsu R928 photomultiplier. Fluorescence lifetimes were measured using a time-correlated single photon counting (TCSPC) technique (Horiba Jobin Yvon) with excitation source NanoLed at 455 nm (Horiba) and impulse repetition rate of 1 MHz at 90° to a TBX-4 detector. The detector was set to 570 nm with a 5 nm band-pass. The instrument was set in the Reverse TAC mode, where the first detected photon represented the start signal by the time-to-amplitude converter (TAC), and the excitation pulse triggered the stop signal. DAS6 decay analysis software was used for lifetime calculation.

RESULTS AND DISCUSSION

Assessment of the Relative Hydrophilicity of Cyanine Dyes. Chart 1 shows the molecular structures of the three cyanine-APTS derivatives employed, which differ only in the number of sulfonic groups on the indoleninic rings. Sulfonic groups are usually inserted to increase the molecular solubility in water,[36] after which the degree of hydrophilicity of the three dyes is expected to progressively decrease from I3BS-APTS to I3NS- APTS. Accordingly, the retention times determined from RP- HPLC analyses were of 8, 24, and 29 min in the order (see Table S1 in the Supporting Information), indicating an increasing affinity for the hydrophobic stationary phase and, consequently, a lower solubility in polar solvents, such as water.

Photophysical Properties of Cyanine-APTS Derivatives. For comparison with the data obtained for dye derivatives in the microemulsion (see the next section), absorption and emission spectra (and related lifetimes) of I3BS-APTS, I3MS- APTS, and I3NS-APTS dissolved in liquid media corresponding to single microemulsion components were also collected. As an example, both kind of data obtained in water are displayed in Figure 1, panels A−C (spectra normalized in intensity), whereas the other absorption and emission spectra are shown in Figure 2 and Figure S1 in the Supporting Information. In general, the absorption profiles exhibit a main peak and two hypsochromic shoulders, with an almost specular counterpart in the emission spectra, with similar positions for the three cyanine-APTS derivatives.

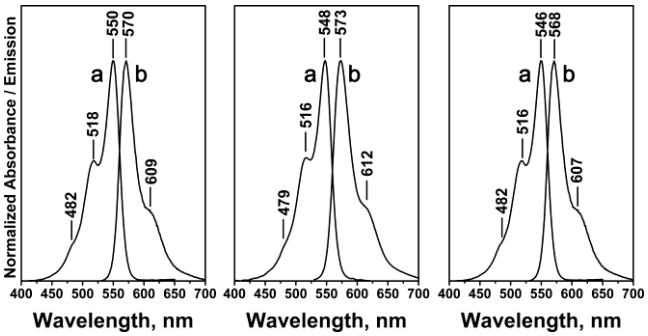

Figure 1. Absorption (curves a) and emission (curves b; λ_{exc}= 500 nm) spectra in water of I3BS-APTS (panel A), I3MS-APTS (panel B) and I3NS-APTS (panel C).

Detailed band assignments can be found in ref 33. Related quantitative features are listed in Table S1 in the Supporting Information.

First Step: Location of Fluorophores in the Initial Microemulsion. Similar spectroscopic measurements were performed for the three cyanine-APTS derivatives in micro- emulsion, before the addition of NH_3 (promoting the hydrolysis of the alkoxysilane moieties) to investigate the location of the fluorophore molecules before the beginning of NPs formation.

The corresponding absorption spectra are compared with those obtained for the cyanine-APTS dissolved in pure components of the microemulsion in Figure 2. The solvatochromic behavior of the indocarbocyanine dyes has been described as nonpolar solvation, since the effect of the solvent is linearly related to the refractive index.[37]

It can be observed that for I3BS-APTS in microemulsion (panel A′) both the main band and the shoulder exhibit the same location as in the spectrum recorded in water solution (panel A). In the case of I3MS-APTS (panel B′), the absorption spectrum is located in an intermediate position with respect to those recorded in water and *n*-hexanol solutions (panel B), whereas for I3NS-APTS (panel C′), the spectrum for the microemulsion is located between the spectra recorded in *n*-hexanol and cyclohexane.

For the emission behavior, similar trends were exhibited by the steady-state spectra (Figure S1 in the Supporting Information). However, the composition of the microemulsion resulted in a molar concentration of cyanine-APTS derivatives (6×10^{-6} mol·L^{-1}) that was high enough to produce a photoemission intensity outside the range where a linear relationship was present between the intensity and the amount of fluorophores, which was limited to 2.5×10^{-6} mol·L^{-1}.[33]

Complementary information was provided by the fluorescence lifetimes (τ_F values in Figure 2; see also Table S1 in the Supporting Information, column 6). By combining the positions of the spectral patterns (which were mainly sensitive to the polarity of the environment) and the photoemission lifetimes (which were sensitive also to differences in the degrees of freedom of fluorophores), the following can be inferred (Scheme 1):

(i) The presence of the two sulfonic groups (I3BS-APTS) resulted in a complete partition in the “water pool” within the reverse micelles. The significantly longer τ_F with respect to the dye dissolved in bulk water indicates a reduced mobility of the H_2O molecules (and, consequently, of the compartmentalized fluorophores) in the water pools within the reverse micelles.

(ii) The presence of a single sulfonic group drove the partition of I3MS-APTS molecules in an environment characterized by an intermediate polarity with respect to water and *n*-hexanol (present as a cosurfactant in the micellar palisade) and a partial loss of molecular degrees of freedom. Thus, it can be proposed that these molecules are preferentially located at the interface between the water pool and the inner side of the surfactant palisade.

(iii) Similar considerations can be made for not-sulfonated I3NS-APTS molecules, which, because of their lower hydrophilicity, should be preferentially located near the outer side of the surfactant palisade toward the oil phase.

Second Step: Behavior of Fluorophores during the Synthesis of Nanoparticles. The formation of the NPs was initiated by adding the aqueous ammonia solution to the reverse microemulsion. Aliquots of the reaction medium were analyzed at increasing time intervals. The absorption and steady-state emission spectra were recorded until the first hour of reaction, after which the increasing turbidity of the medium prevented their measurement. However, during this time interval, no significant changes in the absorption profiles were observed (Figure S2-A in the Supporting Information), whereas some reduction in the emission intensity occurred, which likely resulted from an increase of the scattering of the emitted light from the suspension of the nascent NPs (Figure S2-B in the Supporting Information). This effect did not affect the time- resolved measurements that were carried out during the whole reaction time.

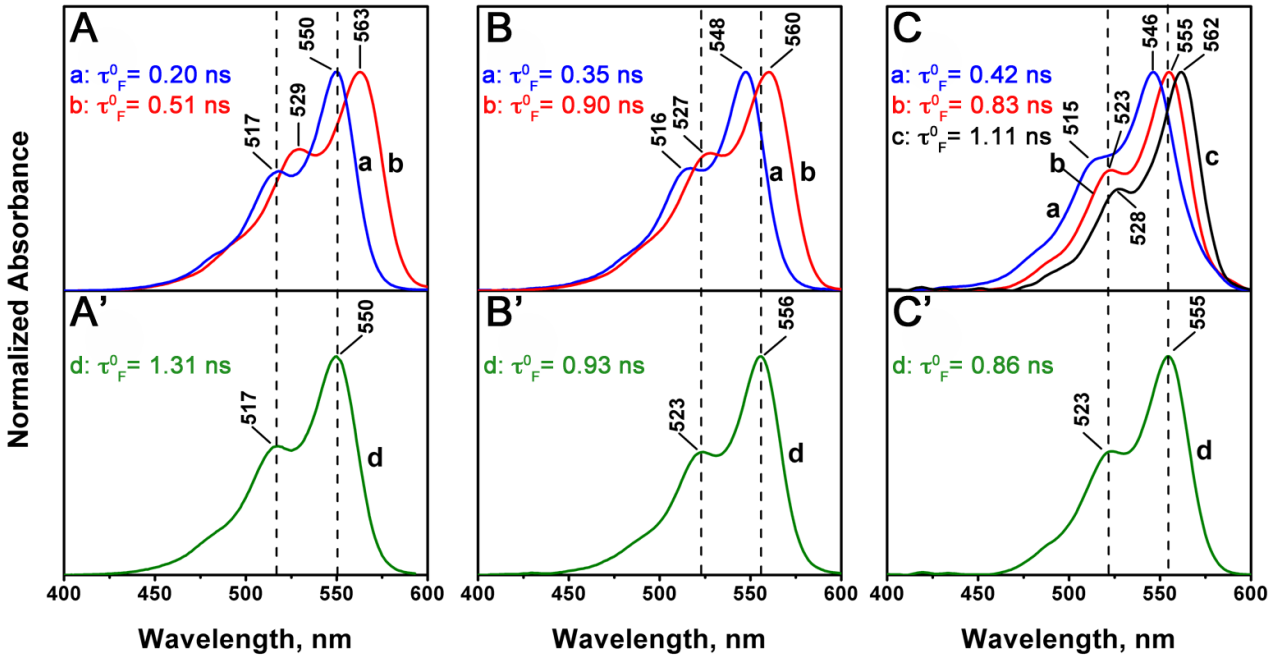

Figure 2. Absorption spectra of I3BS-APTS (panel A and A') I3MS-APTS (panel B and B') and I3NS-APTS (panel C and C') in water ("a" lines, blue), *n*-hexanol ("b" lines, red), cyclohexane ("c" lines, black) and microemulsion ("d" lines, green). I3BS-APTS and I3MS-APTS are almost not soluble in cyclohexane. In each panel the life times obtained in time-resolved photoluminescent measurements are also reported.

Scheme 1. Distribution of the cyanine derivatives in the microemulsion system before the starting of the NPs synthesis.

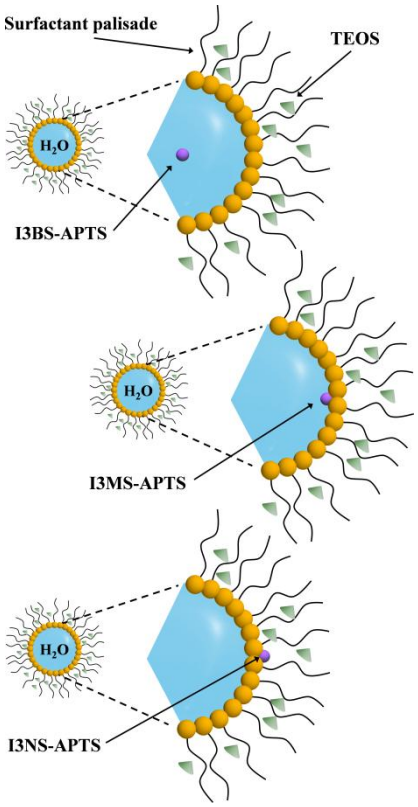

After the reaction was initiated, all systems exhibited two fluorescence lifetimes, and the relative amount of fluorophores exhibiting the shorter lifetime (τ^0_F, similar/coincident with τ_F in the initial microemulsion) progressively decreased in favor of the fluorophores with the longer one, τ^1_F. No significant changes occurred after 16 h, indicating the completion of the process (Table S2 in the Supporting Information). During the reaction, the shorter lifetime (Figure 3)

(i) became progressively longer by ca. 15% in the case of I3NS-APTS.
(ii) remained basically unchanged for I3MS-APTS.
(iii) was shortened by ca. 9% after 4 hours and then increased in some extent with a final decrease by ca. 5% in the case of I3BS-APTS.

Analyses performed after the completion of the reaction (Table 2) indicated that all I3BS-APTS and I3NS-APTS species participated in the formation of the hybrid NPs, and the behaviors described in points i and iii indicated that a portion of the dye molecules associated with the NPs experienced an environment that was not dramatically different from the original molecular medium. In the case of I3MS-APTS, it can be concluded that ca. 17% of the species remained unreacted (Table 2), but after subsequent washing, NPs containing these dyes exhibited an emission decay that still featured a similar short lifetime (Table S3 in the Supporting Information). Also, NPs hybridized with I3MS should then contain a fraction of the dye molecules that experience an environment similar to the parent molecular medium.

For the other population of emitting molecules, their longer τ_F must be related to a close involvement of the cyanine-APTS derivative in the formation of the solid phase, with a consequent loss of molecular mobility. The associated prevention of the interaction with dissolved O_2 should play a minor role because collisional quenching is not particularly effective for fluorophores with lifetimes that are typically shorter than 5 ns.[38a]

The progressive extension of the long τ_F of all types of cyanine-APTS derivatives during the reaction indicates the formation of a progressively more rigid and complete solid environment.

The evolution of the relative amount of cyanine-APTS derivatives with short and long τ_F was monitored throughout the reaction time. Because the two trends are related, for the sake of clarity, only the one associated with the long τ_F, and thus unequivocally related to the nascent solid phase, is reported here (Figure 4). The complete graph, with trends for both τ_F, is displayed in Figure S3 in the Supporting Information. Before proceeding further, it must be recalled that the percentage of I3MS-APTS exhibiting the long τ_F was lower than the percentages recorded for the other two cyanine-APTS derivatives because of the presence of an unreacted fraction that contributed to the complementary fluorophore population with short τ_F. In any case, the more telling information in Figure 4 is provided by the trends of the curves related to the various cyanine-APTS derivatives. During the first hour of the reaction, all systems behaved in a similar way, and

(i) in the case of I3NS-APTS (curve a), the percentage of fluorophores exhibiting the long τ_F monotonically increased up to 12 h of reaction and finally remained almost constant.
(ii) a similar trend was observed for I3MS-APTS (curve b), but with a significantly lower slope over the 1−12 h period.
(iii) in contrast, the relative amount of I3BS-APTS exhibiting the long τ_F remained generally unchanged over the 2−8 h of reaction, increased up to 16 h, and then remained unchanged.

An explanation for these behaviors will be introduced after the presentation of the photoemission properties of the final NPs.

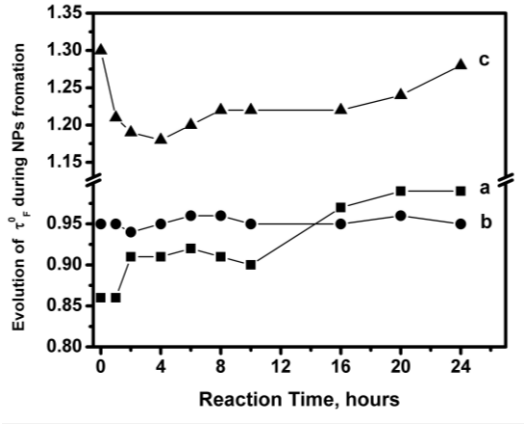

Figure 3. Evolution, along the period required for the formation of the nanoparticles, of the values of the shorter lifetime (τ^0_F): I3NS-APTS (curve a), I3MS-APTS (curve b), and I3BS-APTS (curve c).

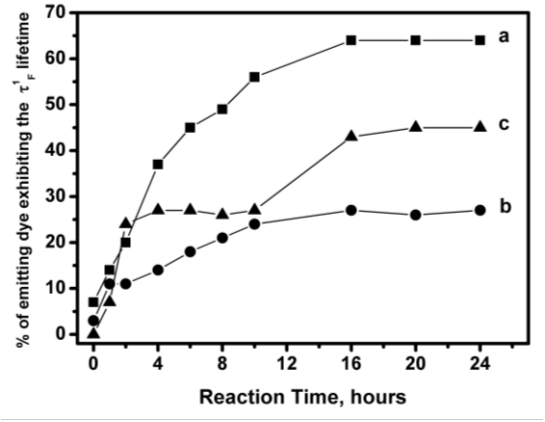

Figure 4. Evolution, along the period required for the formation of the nanoparticles, of the percentage of emitting dyes exhibiting the "longer" lifetime τ^1_F: I3NS-APTS (curve a), I3MS-APTS (curve b), and I3BS- APTS (curve c).

Table 2. Quantitative features of Cyanine-NPs syntheses

Cyanine-APTS derivative	Cyanine-APTS molecules used (moles)	Cyanine molecules entrapped (moles,%)	NPs obtained (number)	Cyanine molecules per NP (number)
I3BS-APTS	$5.65 \cdot 10^{-7}$	$5.65 \cdot 10^{-7}$, 100%	$3.08 \cdot 10^{15}$	~110
I3MS-APTS	$5.65 \cdot 10^{-7}$	$4.69 \cdot 10^{-7}$, 83%	$3.08 \cdot 10^{15}$	~ 86
I3NS-APTS	$5.65 \cdot 10^{-7}$	$5.65 \cdot 10^{-7}$, 100%	$3.08 \cdot 10^{15}$	~110

Third Step: Photoemission Properties of the Cyanine- Doped SiO_2 NPs in the Final Form. After the reaction was completed, the hybrid NPs were recovered from the liquid medium as indicated in the Experimental Section. On the basis of the amounts of TEOS and cyanine-APTS species in the liquid medium before and after NPs formation and the estimation of the number of NPs produced (see below), the average number of cyanine molecules per nanoparticle was calculated for the three materials (Table 2). The inductively coupled plasma (ICP)-mass analyses of the medium indicated that ca. 90% of the TEOS was converted to silica; further UV−vis analyses of the reaction liquids indicated the absence of I3BS-APTS and I3NS-APTS unreacted molecules (which were completely associated to the solid phase) and the presence of ca. 17% of the initial amount of I3MS-APTS. The reason for the incomplete association of these species with the solid NPs is the subject of an extension of this work. Using the average volume (derived from the NPs size distribution, Figure S4 in the Supporting Information) and density of the NPs, the number of NPs and the average number of cyanine molecules per NP were then calculated.

It is worth noting that, because of the narrowness of the size distribution, the average properties of the systems are significantly representative of the properties of each NP.

The recovered hybrid NPs were suspended in the appropriate amounts of liquids with different polarities to assess the possible presence of fluorophores attached to the surface of the nanoparticles. The requirement of attaining a stable suspension limited the choice of liquid media to H_2O, CH_3OH, and CH_3CH_2OH. The suspensions that were sufficiently concentrated to produce a detectable absorbance exhibited a scattering that was too high to permit measurements in the transmission mode; thus, the excitation (λ_{em} = 600 nm) and emission spectra (λ_{ex} = 520 nm) were collected. For the sake of brevity, only the excitation data are displayed here (Figure 5), whereas the emission data are reported in Figure S5 in the Supporting Information.

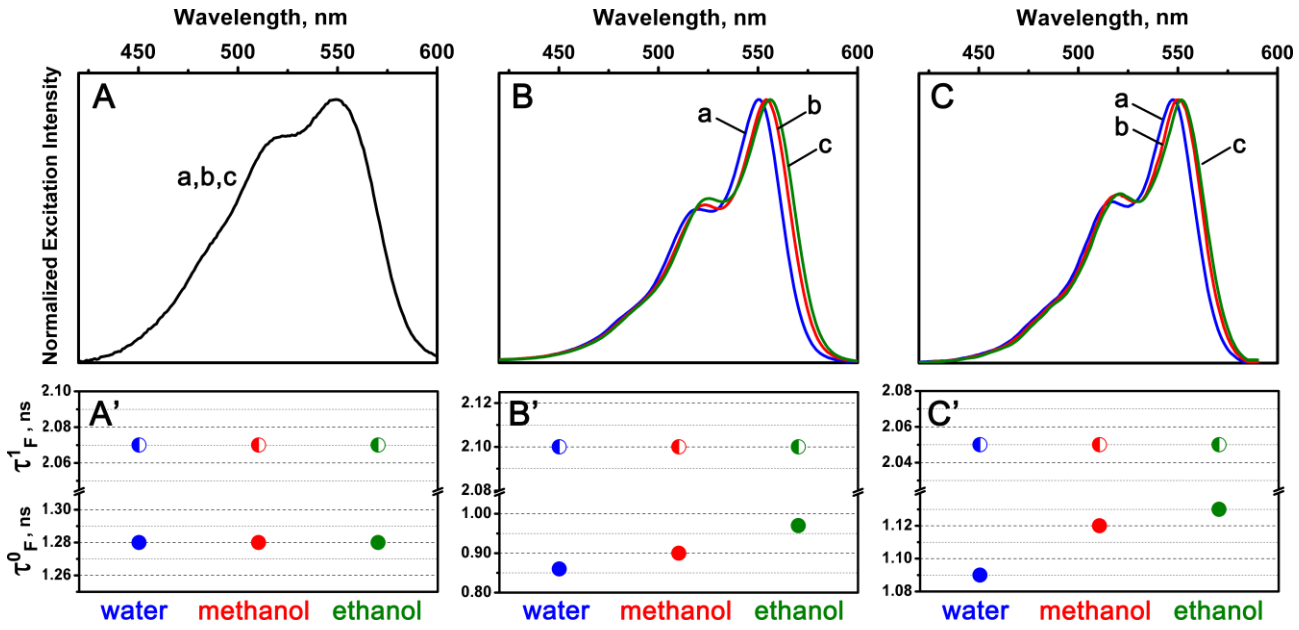

Figure 5. Top: excitation (λ_{em}= 600 nm) spectra of I3BS-NPs (panel A), I3MS-NPs (panel B) and I3NS-NPs (panel C) in water (blue, curve a), methanol (red, curve b) and ethanol (green, curve c).In the case of I3BS-NPs, all curves resulted overlapped. Bottom: values of τ^0_F (solid symbols) and τ^1_F (half solid symbols) of I3BS-NPs (panel A'), I3MS-NPs (panel B') and I3NS-NPs (panel C') in water (blue), methanol (red) and ethanol (green).

The decrease in the polarity of the suspension medium did not affect the spectral profile of the I3BS-NPs (panel A), which indicates the complete inclusion of the fluorophores within the NPs. Conversely, a slight downshift occurred in the spectra of the I3MS-NPs and I3NS-NPs (Figure 5, panels B and C, respectively), which indicates the presence of at least a portion of the fluorophores on the surface of the NPs. A confirmation and more quantitative evidence for this partition was provided by the complementary time-resolved emission measurements (Figure 5, bottom panels and Table S3 in the Supporting Information); when the polarity of the suspending medium was changed, both lifetimes contributing to the decay of the emission of I3BS-NPs remained unchanged, whereas in the case of I3MS-NPs and I3NS-NPs, the shorter τ_F was affected.

It is thus reasonable to infer that the fluorophores in I3MS- NPs and I3NS-NPs exhibiting the short τ_F should be located on the surface of the nanoparticles, whereas in the case of I3BS-NPs, all cyanines are embedded in the silica matrix. In this case, the presence of two lifetimes indicates that the siliceous network can form two types of structures around the fluorophores. With regard to the steady-state spectra, the solvatochromic behavior exhibited by the excitation spectra of the first two materials should then result from the superposition of a spectral profile insensitive to the change in the suspending medium and a second slightly shifted profile that depends on the polarity of the solvent.

Focusing on the systems containing I3BS-APTS molecules, it must be noted that the profile of the I3BS-NPs excitation spectrum (Figure 5A) appeared different with respect to the absorption spectra of I3BS-APTS in solution (Figures 2A, A′), whereas such a difference was not observed in the case of nanoparticles and solutions containing I3MS-APTS and I3NS-APTS molecules. Moreover, no significant differences were observed between the emission spectrum of I3BS-NPs and the spectra of the fluorophore in the parent-free molecular form (see Figure S5 in the Supporting Information and Figure 1). Similar behavior was observed in previous studies of another type of cyanine derivative, in which all molecules were ultimately entrapped in the silica matrix.[33] Thus, by assuming that the sub-bands in the absorption/excitation molecules result from the vibronic structure,[38b,39–41] the present results confirm that the complete entrapment of cyanine molecules in a silica matrix can affect the electronic transition to different vibrational levels of the excited state.

Analysis of the Quantitative Photoemission Behavior of Cyanine−Silica Hybrid NPs. The emission intensity of the produced hybrid NPs was then explored through the preparation of a series of aqueous suspensions with known amounts of hybrid NPs. As reported in a previous study,[33] for NP concentrations <2.5 × 10^{13} NPs L^{-1}, the photoluminescence intensity and fluorophore concentration exhibit a highly linear relationship. Water was used as the suspending medium because of the high dispersibility of the hybrid NPs in such liquids and in view of the possible applications of these materials in life science.[42] For the sake of comparison, aqueous solutions of the cyanine-APTS derivatives in the same concentration range were also prepared. The linear emission intensity/cyanine concentration trends obtained for the fluorophores in molecular solutions or associated with the NPs were then compared (Figure 6).

A nearly complete quenching of the fluorescence occurred for I3BS-APTS entrapped in the silica matrix (panel A), whereas the association with NPs resulted in an increase in emission intensity for I3MS-APTS that occurred to an even greater extent for I3NS- APTS (panels B and C, respectively). Separate experiments confirmed the resistance of the three types of cyanine to the basic conditions present in the reverse micelles during reaction; thus, the poor emission of the I3BS-APTS should result from a severe decrease in the absorption coefficient and/or an extensive aggregation of such fluorophores during NP formation.

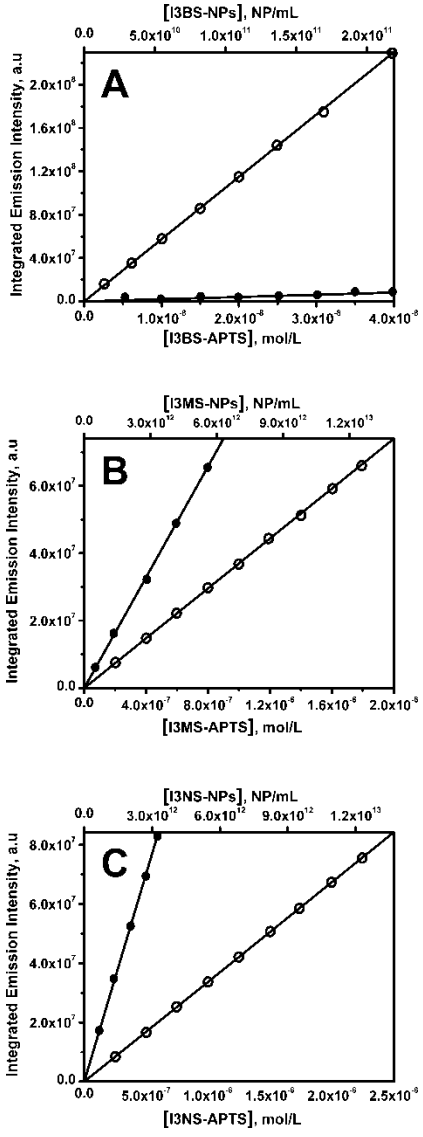

Figure 6. Comparison of the integrated emission intensities (λ_{ex}= 520 nm) at different concentrations of hybrid fluorescent NPs in water suspensions (full symbols) and the correspondent cyanine-APTS in water solutions (empty symbols). Panel A: I3BS-NPs/I3BS-APTS; Panel B: I3MS-NPS/I3MS-APTS; Panel C: I3NS-NPs/I3NS-APTS.

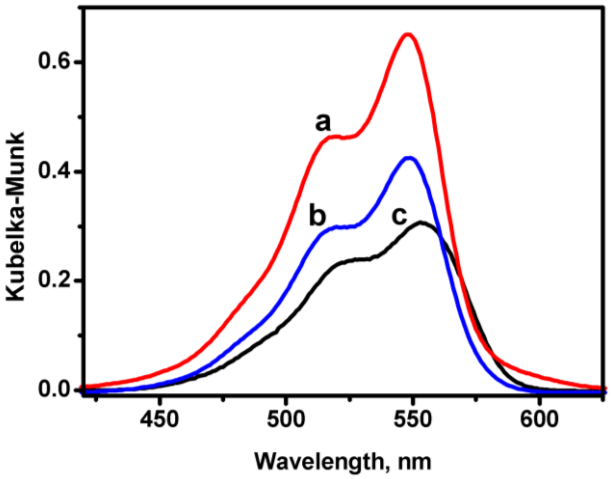

Figure 7. Comparison of the DR-UV-Vis spectra of I3NS-NPs (red, curve a), I3MS-NPs (blue, curve b), I3BS-NPs (black, curve c).

The possibility of differences in the absorption coefficient among the three types of cyanines when associated with NPs or dissolved in solution (Table S1 in the Supporting Information) was assessed by collecting the absorption spectra of dry hybrid-NPs powders in the diffuse-reflectance mode (Figure 7). In all cases, the spectra obtained after the conversion of the original reflectance data by using the Kubelka−Munk function exhibited a maximum value <1, which represents the upper limit for the application of such a function to obtain a linear relationship between the absorption intensity and concentration of the absorptive species.[43] Furthermore, the similarity of the NPs constituting the three materials in terms of size and density indicates that the NPs should exhibit similar scattering behavior.

The data were normalized with respect to the number of cyanine molecules per nanoparticle (Table 2), and the following ratios among the integrated absorption intensity of the three materials were obtained: I3NS-NPs/I3MS-NPs/I3BS-NPs = 1/0.83/0.37. The comparison of such values with the ratios between the decadic absorption coefficients measured for the cyanine-APTS species in solution (from Table S1 in the Supporting Information: I3NS-NPs/I3MS-NPs/I3BS-NPs = 1/0.87/0.80) indicated that a decrease of ca. 50% of the absorption capability of I3BS occurred when associated with the silica matrix, but this loss was not sufficient to explain the nearly complete absence of photoluminescence exhibited by I3BS-NPs.

As a second point, the steady-state and time-resolved photo- emission data were quantitatively treated to evaluate (in relative terms) the changes in the quantum yields of fluorophores when transitioning from the solute state in a liquid medium to the state of association with a silica nanoparticle.

As for the emission intensity measured through steady-state experiments, the following relationship between the intensity of the emission of a photoluminescent molecular system (Q) under excitation conditions (I_0), molar decadic absorption coefficient (ε), optical path (b), molar concentration (c), and photoemission quantum yield (Φ) can be written:

$$Q = I_0(\varepsilon bc)\,\Phi \qquad (1)$$

It can be inferred that the different slopes between the linear trends in each panel of Figure 6 are proportional to a difference in the quantum yield (Φ) of the fluorophores when in solution or associated with NPs and, consequently, the ratio between the two slopes corresponds to the ratio between the quantum yields. It is important to note that, in eq 1, all molecules responsible for the fluorophore concentration (c) are assumed to be photoluminescent. In the present case, this condition is expected for the solutions of fluorophores, whereas NPs can contain photoemitting and not-

photoemitting species. Hence, when eq 1 is applied to hybrid NPs, the term Φ represents a photoemission quantum yield averaged over ALL cyanine molecules, independent of their actual contribution to the photoemission; this term will be hereafter referred to as Φ_{ALL}. On the basis of these considerations, the relative change in the photoemission quantum yield passing from the fluorophores in solution (SOL) to fluorophores associated with NPs can be calculated as follows:

$$\text{Relative change } \Phi_{ALL} = [\text{slope Eq.}(1)_{NPs}]/[\text{slope Eq.}(1)_{SOL}] \quad (2)$$

The values obtained by applying this equation are listed in Table 3, column 1.

Table 3. Relative changes in photoemission quantum yield (Φ) exhibited from the fluorophores when in solution or associated with NPs.

Cyanine	Relative change in Φ_{ALL} (Cy-NP) /(Cy in solution)	Relative change in Φ_{EM} (Cy-NP) /(Cy in solution)	Percentage of Photoluminescent Cyanine molecules (%)
I3BS	0.04	5.6	0.7
I3MS	2.7	4.3	63
I3NS	4.37	4.42	100

[a] Φ_{ALL} (see Eq. 2): relative quantum yield averaged over all cyanine molecules present in the solutions or in the NPs suspensions; Φ_{EM} (see Eq. 3): relative quantum yield of cyanine molecules actually emitting (the only ones exhibiting a photoemission lifetime). The percentage of photoluminescent cyanine molecules resulted from the ratio between the relative changes in Φ_{ALL}/ Φ_{EM}.

The changes in photoemission intensity as a combination of the increase and decrease in the quantum yield of fluorophores that underwent different fates when associated with NPs can be evaluated by analyzing the emission lifetimes. Indeed, by assuming that most of the possible gain in Φ after the entrapment/association with silica matrix results from a decrease in the rate of nonradiative decay processes, the relative change in Φ exhibited by the fraction of cyanine molecules that were actually photoluminescent when hybridized with silica can be determined by rationing their photoemission lifetimes [hereafter: $\tau_{F\ NPs}$] with respect to the photoemission lifetime τ_F that they exhibited in solution [hereafter: $\tau_{F\ SOL}$]. In the presence of more than one population of fluorophores, each with a specific photoemission lifetime, the average relative change in Φ of the emitting molecules can then be obtained by applying the following formula:

$$\text{Relative change } \Phi_{EM} = \sum x_i(\tau_F i)_{NPs} / (\tau_F i)_{SOL} \quad (3)$$

where Φ_{EM} indicates that only emitting dye molecules (which exhibit an emission lifetime) are considered, and a summation is made over the i populations that accounts for the x_i fraction of fluorophores contributing to the overall time decay.

The values of the relative changes in Φ_{EM} calculated for the three systems are listed in Table 3, column 2, and clearly indicate that, on average, all types of emitting cyanine molecules associated with/entrapped in the silica matrix exhibited an increase in quantum yield. It must be considered that the changes in Φ_{ALL} and in Φ_{EM} should be coincident if all fluorophores present in the NPs contribute to the photoemission. If not, the percentage of fluorophores actually producing the photoemission with respect to their total amount can be derived from the ratio between Φ_{EM} and Φ_{ALL} (Table 3, column 3). By adopting this criterion, a very low value was obtained for I3BS, whereas a value of close to 100% was

calculated for I3NS, thereby indicating the high effectiveness of the association of these molecules with the NPs. In the case of I3MS, the calculation revealed that ca. 40% of the cyanine molecules associated with NPs were quenched.

Thus, it can be inferred that a higher hydrophilicity of the cyanine derivative added to the reverse microemulsion results in a higher possibility of aggregation during the formation of NPs, with a consequent, even quite severe, loss of photoemission efficiency of the fluorophores associated with the silica matrix (Scheme 2).

Dispersion vs Aggregation of Fluorophores during NP Formation. On the basis of the foregoing statement, it is now possible to analyze the data in Figure 4 to elucidate other aspects of the processes resulting in the aggregation/dispersion of the more/less hydrophilic fluorophores in the silica matrix. As a preliminary step, it may be useful to recall that the reaction pathway resulting in the formation of silica NPs via the reverse- microemulsion method (general reaction scheme S1 in Supporting Information) involves, in addition to TEOS partition and hydrolysis, nucleation and particle growth, the dissolution of the nuclei and intermicellar contacts with consequent molecular exchange and aggregation of nuclei. It has been estimated that one final silica particle is produced out of 104−106 micelles.[44] In particular, the intermicellar exchange/matter aggregation are expected to occur to a significant extent (i.e., at a rate greater than or equal to a factor of 30 with respect to the diffusion-controlled collision rate) at a high $[H_2O]/[surfactant]$ ratio,[44] as in the present case, where $[H_2O]/[TX\text{-}100] = 10$.

Furthermore, the presence of TEOS $[Si(OR)_4]$ must be considered: such molecules, which are not amphiphilic, are compartmentalized in the bulk oil phase but, when hydrolyzed, are translocated to the micellar phase.[44] Because the tendency of solute molecules to partition to an aqueous phase depends on their hydrophilicity, it is expected that the $Si(OR)_3(OH)$ species would be located in the palisade surfactant layer and $Si(OH)_4$ in the water pool. Thus, the species associated with the micelles before hydrolysis will generally be the cyanine-APTS derivatives (see above), but after the addition of NH_3 and the consequent initiation of TEOS hydrolysis, the micelles will become populated by $Si(OR)_{4-n}(OH)_n$ $(4 > n > 1)$ species that, on the basis of the huge amounts of TEOS with respect to dyes, will become the most abundant. As reported in the section First Step, I3MS-APTS and I3NS-APTS were also found to be located in the palisade before the admission of ammonia. However, after the hydrolysis of the APTS moiety, the translocation in the water pool should occur at a lower rate than that of the species derived from TEOS because of the poorly hydrophilic character of the cyanine structure linked to the hydrolyzed APTS.

Thus, having established that the I3BS-APTS derivative underwent a significant aggregation during the formation of NPs, the flatness of the related curve in Figure 4 between 2 and 10 h of reaction might result from the establishment of a steady-state condition between the formation of nuclei containing isolated I3BS-APTS (thus fluorescent and exhibiting a long lifetime) and their evolution in structures containing cyanine molecules that undergo concentration quenching. Such

Scheme 2. Distribution of the cyanine derivatives in the final hybrid fluorescent NPs

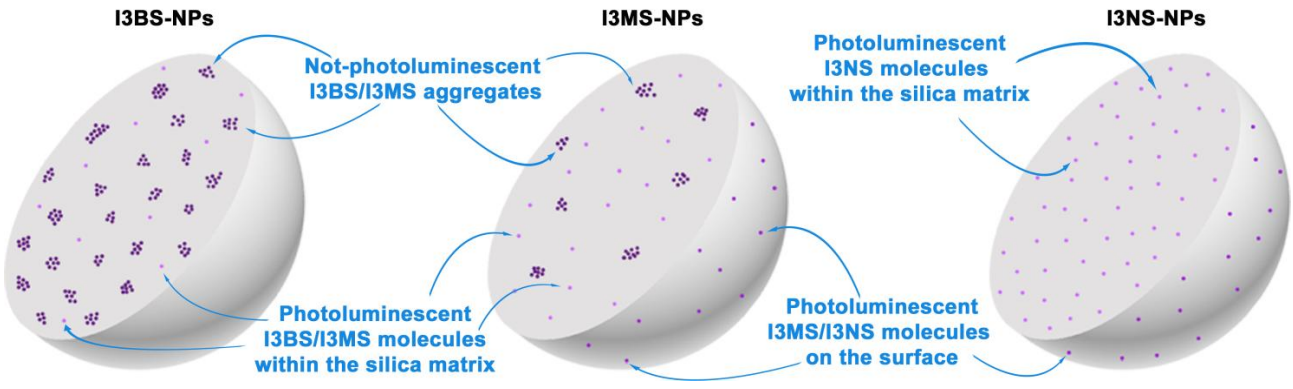

an evolution might be related to the involvement of matter exchange/mixing with other micelles containing I3BS-APTS species located in the water pool. These latter species can condense, through the hydrolyzed APTS moiety, with the nuclei already bearing a cyanine molecule, or the nuclei could undergo dissolution during exchange/ mixing, thereby allowing the originally entrapped I3BS-APTS species to interact with those present in the water pool of the other micelles.

Such a phenomenon should play an increasingly minor role as the hydrophilicity of the cyanine-APTS species decreases, thereby resulting in a preferential partition in the surfactant palisade of the micelles, which is apparently less involved in the matter exchange/mixing with other micelles. Hence, the trends exhibited by curves a and b in Figure 4, which are related to I3NS-APTS and I3MS-APTS, respectively, suggest that the involvement of such species in the growth of nanoparticles occurred after the formation of silica subparticles that were larger in size and more stable than the nuclei.

CONCLUSIONS

The data presented demonstrate that the reverse-microemulsion method can be usefully employed not only to produce dye−silica hybrid nanoparticles that are highly uniform in size but also to design a proper distribution of fluorescent guests in the silica matrix. As a consequence, all organic molecules can be exploited to maximize the increase in photoemission intensity resulting from the loss of molecular degrees of freedom. To attain such a target, fluorophores with a low hydrophilicity must be selected because of their permanence in an unaggregated form during the growth of the nanoparticles. This is a distinct feature with respect to the behavior exhibited by nonpolar fluorophores when used for the production of dye -doped silica nanoparticles by the Stöber −Van Blaaderen method, which results in a spontaneous accumulation in the core.[28]

AUTHOR INFORMATION

Corresponding Author

*Email: gianmario.martra@unito.it; gabriele.alberto@unito.it.

Notes

The authors declare no competing financial interest.

ACKNOWLEDGMENTS

The research was funded by Regione Piemonte (Misura I.1.3 “Poli di Innovazione”-I Programma, Polo: Biotecnologie e Biomedicale; Project BANP). G.A. is recipient of a fellowship by ASP-Torino.

REFERENCES

(1) Paquet, C.; Kumacheva, E. Materials Today 2008, 11, 48.

(2) Fang, X.S.; Bando, Y.; Gautam, U.K.; Zhai, TY.; Zeng, H.B.; Xu, X.J.; Liao, M.Y.; Goldberg, D. Crit. Rev. Solid State Mater. Sci. 2009, 34, 190.

(3) Kalinowski, J.; Fattori, V.; Cocchi, M.; Gareth Williams, J.A. Coord. Chem. Rev. 2011, 255, 2401.

(4) Uthirakumar, P.; Lee, Y.S.; Suh, EK.; Hong, C.H. J. Lumin. 2008, 128, 287.

(5) Sailor, M.J.; Wu, E.C. Adv. Funct. Mater. 2009, 19, 3195.

(6) Somers, R.C.; Bawendi, M.G.; Nocera, D.G. Chem. Soc. Rev 2007, 36, 579.

(7) Coto-Garcia, A.M.; Sotel-Gonzalez, E.; Fernandez-Arguelles, M.; Pereiro, R.; Costa-Fernandez, J.M.; Sanz-Medel, A. Anal. Bioanal. Chem. 2011, 399, 29.

(8) Boisselier, E.; Astruc, D. Chem. Soc. Rev. 2009, 38, 1759.

(9) Liu, L.; Gill, S.K.; Gao, Y.; Hope-Weeks, L.J.; Cheng, K.H. Forensic Sci. Int. 2008,176, 163.
(10) Theaker, B.J.; Hudson, K.E.; Rowell, F.J. Forensic Sci. Int. 2008, 174, 26.
(11) Resch-Genger, U.; Grabolle, M.; Cavaliere-Jaricot, S.; Nitschke, R.; Nann, T. Nat. Methods 2008, 5, 763.
(12) Medintz, I.L.; Uyeda, H.T.; Goldmn, E.R.; Mattoussi, H. Nat. Mater. 2005, 4, 435.
(13) Fercher, A.; Borisov, S.M.; Zhdanov, A.V.; Klimant, I.; Papkovsky, D.B. ACS Nano 2011, 5, 5499.
(14) Tong, R.; Coyle, V.J.; Tang, L.; Barger A.M.; Fan, T.M.; Cheng J. Microsc. Res. Tech. 2010, 73, 901.
(15) Zhao, X.; Bagwe, R.P.; Tan, W. Adv. Mater. 2004, 16, 173.
(16) Lian, W.; Litherland, S.A.; Badrane, H.; Tan, W.; Wu, D.; Baker, H.V.; Gulig, P.A.; Lim, D.V.; Jin, S. Anal. Biochem. 2004, 334, 135.
(17) Gianotti, E.; Bertolino, C.A.; Benzi, C.; Nicotra, G.; Caputo, G.; Castino, R.; Isidoro, C.; Coluccia, S. Appl. Mater. Interfaces 2009, 1, 678.
(18) Abarkan, I.; Doussineau, T.; Smaïhi, M. Polyhedron 2006, 25, 1763.
(19) Arriagada, F.J.; Osseo-Asare, K. J. Colloid Interface Sci. 1995, 170, 8.
(20) Huang, S.; Li, R.; Qu, Y.; Schen, J.; Liu, J. J. Fluoresc. 2009, 19, 1095.
(21) Bharali, D.J.; Klejbor, I.; Stachowiak, E.K.; Dutta, P.; Roy, I.; Kaur, N.; Bergey, E.J.; Prasad, P.N.; Stachowiak, M. PNAS 2005, 102, 11539.
(22) Rosi, N.L.; Mirkin, C.A. Chem Rev. 2005, 105,1547.
(23) Santra, S.; Zhang, P.; Wang, K.; Tapec, R.; Tan W. Anal. Chem. 2001, 73, 4988.
(24)Van Blaaderen, A.; Vrij, A.J. Langmuir 1992, 8, 2921.
(25) Van Blaaderen, A.; Vrij, A. J. Colloid Interface Sci. 1993, 156, 1.
(26) Stöber, W.; Fink, A.; Bohn, E. J. Colloid Interface Sci. 1968, 26, 62.
(27) Rampazzo, E.; Bonacchi, S.; Montalti, M.; Prodi, L.; Zaccheroni, N. J. Am. Chem. Soc. 2007, 129, 14251.
(28) Larson, D.R.; Ow, H.; Vishwasrao, H.D.; Heikal, A.A.; Weisner, U.; Webb, W.W. Chem. Mater. 2008, 20, 2677.
(29) Osseo-Asare, K.; Arriagada, F.J. J. Colloid Interface Sci. 1999, 218, 68.
(30) Osseo-Asare, K.; Arriagada, F.J. Colloids Surf. 1990, 50, 321.
(31) Bagwe, R.P.; Yang, C.; Hilliard, L.R.; Tan, W. Langmuir 2004, 20, 8336.
(32) Mishra, A.; Behera, R.K.; Behera, P.K.; Mishra, B.K.; Behera, G.B. Chem. Rev. 2000,100, 1973.
(33) Alberto, A.; Miletto, I.; Viscardi, G.; Caputo, G.; Latterini, L.; Coluccia, S.; Martra, G. J. Phys. Chem. C 2009, 113, 21048.
(34) Bonacchi, S.; Genovese, D.; Juris, R.; Montalti, M.; Prodi, L.; Rampazzo, E.; Zaccheroni, N. Angew. Chem. Int. Edition 2011, 50, 4056.
(35) Santra S.; Wang, K.; Tapec, R.; Tan, W. J. Biomed. Opt. 2001, 6, 160.
(36) Waggoner, Bioconjugate Chemistry, Volume 4 (2), 1993
(37) Bertolino, C.A.; Ferrari, A.M.; Barolo, C.; Viscardi, G.; Caputo, G.; Coluccia, S. Chem. Phys. 2006, 330, 52.
(38) Lackowicz, J.R. Principles of Fluorescence Spectroscopy 3rd ed, Springer Publishing, Singapore, 2006; a) chapter 19, p 629; b) chapter 1, pp7-8.
(39) Kachkovski, A.D. Dyes Pigments 1994, 24, 171.
(40) Baraldi, I.; Caselli, M.; Momicchioli, F.; Ponterini, G.; Vanossi, D. Chem. Phys. 2002, 275, 149.
(41) Mustroph, H.; Stollenwerk, M.; Bressau, V. Angew. Chem., Int. Ed 2006, 45, 2016.
(42) Miletto, I.; Gilardino, A.; Zamburlin, P.; Dalmazzo, S.; Lovisolo, D.; Caputo, G.; Viscardi, G.; Martra, G. Dyes Pigments. 2010, 84, 121.
(43) Kortüm G. Reflectance Spectroscopy, Springer-Verlag, New York, 1969.
(44) Arriagada, F.J.; Osseo-Asare, K. Colloids Surf. A 1999, 154, 311.